



Cite this: DOI: 10.1039/c9dt00452a

Synthesis and characterization of aminopyridine iron(II) chloride catalysts for isoprene polymerization: sterically controlled monomer enchainment†

Chuyang Jing,^{‡a,b} Liang Wang,^{‡a} Qaiser Mahmood,^a Mengmeng Zhao,^a
Guangqian Zhu,^{a,b} Xianhui Zhang,^{a,b} Xiaowu Wang^{id}*^a and Qinggang Wang^{id}*^a

In this study, a series of 2-R-6-(1-(alkylamino)methyl)pyridine-iron complexes [alkyl: (CPh₃) **Fe1_H**; (CHPh₂) **Fe2_H**; (CHPh₂) **Fe3_{Me}**; (CHMePh) **Fe4_H**; (CH₂Ph) **Fe5_H**; (CHMe₂) **Fe6_H**; (C₆H₁₁) **Fe7_H**; (CH₂(4-OMe)Ph) **Fe8_H**; (CH₂(4-CF₃)Ph) **Fe9_H**; (CH₂(2,4,6-Me₃)Ph) **Fe10_H**; (CH₂Ph) **Fe11_{Me}**] were synthesized and well characterized by ATR-IR spectroscopy, HRMS spectroscopy and elemental analysis. In addition, **Fe3_{Me}**, **Fe4_H**, **Fe7_H** and **Fe11_{Me}** were characterized by X-ray diffraction analysis: **Fe3_{Me}** and **Fe11_{Me}** adopted distorted tetrahedral geometries in the solid state while **Fe4_H** and **Fe7_H** were found in dimeric or polymeric forms respectively in which chlorides acted as bridging ligands. The catalytic capacities of these iron complexes were investigated for isoprene polymerization. Upon activation with a MAO cocatalyst, the catalytic activities of complexes varied as a function of the steric and electronic influences of substituents. In general, the catalysts bearing the least steric groups and electron-withdrawing groups exhibited relatively high activities. An outstanding activity of $190.6 \times 10^4 \text{ g} \cdot \text{mol}^{-1} \cdot \text{h}^{-1}$ was obtained by **Fe5_H** [CH₂Ph]. Moreover, changes in the steric hindrance around the metal center showed a notable effect on the selectivity of monomer enchainment. In particular, most of the polymers obtained by these complexes bearing flexible frameworks were in favor of 3,4-enchainment.

Received 31st January 2019,

Accepted 26th April 2019

DOI: 10.1039/c9dt00452a

rsc.li/dalton

Introduction

Polyisoprene is experiencing ever-growing demands for its applications in tyres, gloves, tubes, shape memory and the medicinal industries.^{1,2} Indeed these materials are replacing the natural rubber due to their excellent flexible and ductile properties similar to the vulcanized rubber, and their processing and recycling properties also make them superior over natural rubber. In principle, isoprene polymerization has four types of monomer enchainments namely *cis*-1,4- and *trans*-1,4-, 1,2- and 3,4-. The degree and type of enchainment of the monomer define the end-use applications of the polymer.^{3,4} More specifically, polyisoprene with side-chain olefins result-

ing from 3,4-enchainment of the monomer is an important component in synthetic rubber upon selective crosslinking which can be beneficial for preventing abrasion of tyres. These materials could also find application in high performance rubbers with wet-skid resistance and low-rolling resistance tread.^{3,5} Although polymerizations mediated by early transition metal catalysts or conventional Ziegler-Natta catalysts have been developed for more than 60 years,^{6,7} there have been exciting recent advances in terms of late transition metal catalyzed polymerization. Since the discovery of α -diimino-Ni(II)/-Pd(II)^{8,9} in 1995 and bis(imino)pyridine-Fe(II)/-Co(II)^{10,11} catalysts in 1998 for olefin polymerization, late transition metal catalysts have attracted great attention from both academia and industries.¹²⁻¹⁵ Up to now, most studies have been focused on ethylene oligo/polymerization using late transition metal precatalysts,¹⁶⁻²⁰ in particular *N,N,N*-tridentate cobalt²¹⁻²³ and iron²⁴⁻²⁸ and *N,N*-bidentate nickel²⁹⁻³³ and palladium³⁴⁻³⁷ complexes. Among them, iron complexes have been found as highly active precatalysts for ethylene oligo/polymerization and featured an expedient preparation and an eco-friendly and abundant metal.^{38,39} In the last few decades, well-defined iron based catalysts have also been developed for regio- and/or stereoselective polymerization of dienes.^{40,41} *N,N*-

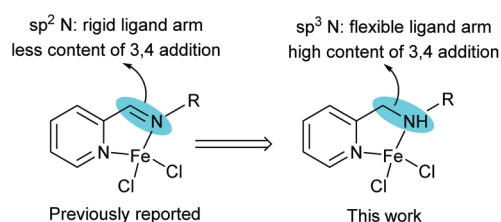
^aKey Laboratory of Biobased Materials, Qingdao Institute of Bioenergy and Bioprocess Technology, Chinese Academy of Sciences, Qingdao, 266101, China.
E-mail: wangxw@qibebt.ac.cn, wangqg@qibebt.ac.cn

^bCenter of Materials Science and Optoelectronics Engineering, University of Chinese Academy of Sciences, Beijing, 100049, China

† Electronic supplementary information (ESI) available. CCDC 1884491 (**Fe7_H**), 1884670 (**Fe3_{Me}**), 1884671 (**Fe11_{Me}**) and 1884672 (**Fe4_H**). For ESI and crystallographic data in CIF or other electronic format see DOI: 10.1039/c9dt00452a

‡ These authors contributed equally.

Chelates such as α -diimine,^{42,43} (imino)pyridine^{44–46} and bipyridine^{47–50} were elegant examples in the field of diene polymerization. However, low productivity, poor selectivity and low molecular weight of the resultant polydiene polymer were characteristics of iron mediated diene polymerization. In spite of these, there has been considerable and growing interest to develop new ligand motifs for improving the catalytic performance of the iron based catalysts. Some elegant examples of iron catalysts for isoprene polymerization have been developed by Ritter⁴⁴ and Chen⁴⁵ groups. The resulting polyisoprene possessed a high content of *cis*-1,4 motifs with a low amount of side-arm olefin groups. Very recently, our group focused on establishing the correlations of the ligand architecture of iron based catalysts with their catalytic performance for isoprene polymerization. We observed that the introduction of an electron-withdrawing group (CF₃) into the *N*-aryl imines of iminopyridine-iron complexes showed a positive effect on the catalytic performance in terms of activity.⁴ Subsequent work expanded the ligand backbone to an iminoimidazole motif⁵¹ and the iron salt was extended to Fe(acac)₂.⁵² Other studies have shown that the mode of coordination with the metal center plays a crucial role in controlling the catalytic performance:^{53–55} the modes of coordination such as amide-metal (C–(R)N[–] → M) and imine-metal (C=N → M) (including nitrogen containing heterocycles such as pyridine) have been well studied. However, amine-metal (C–(R)N → M) with coordination of an amine to iron metal was rarely been explored toward isoprene polymerization. It is tempting to explore the different modes of coordination of the side arm to concurrently achieve high activities and subtle control over the microstructure of the polymer.^{56–58}



Scheme 1 Structural variations in imino- and aminopyridine-iron(II) pre-catalysts.

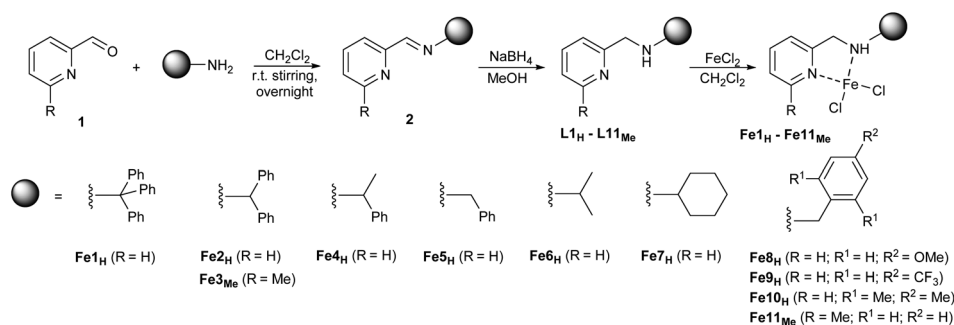
In this work, we explored a new family of aminopyridine-iron complexes as precatalysts for isoprene polymerization. By reducing the imine bond of the iminopyridine ligand framework, we prepared a series of aminopyridine-iron catalysts and additionally probe the effects of different steric and electronic substituents toward isoprene polymerization (Scheme 1). A detailed polymerization study was performed and the influences of different reaction parameters such as Al/Fe and IP/Fe ratios, reaction temperature and run time were also ascertained. In addition to the catalytic investigation and polymer characterization, synthesis and characterization of ligands and their complexes were reported.

Results and discussion

Synthesis and characterization of ligands and their iron(II) complexes

A series of 2-R-6-(1-(alkylamino)methyl)pyridine ligands bearing different alkyl substituents have been prepared using a two-step procedure as represented in Scheme 2. The intermediate compounds **2** could be obtained by the Schiff base condensation of (2-methyl)picolinaldehyde with the corresponding anilines under mild conditions in good to excellent yields. The efficiency of this reaction was substantially improved by performing the reaction in the presence of activated 4 Å molecular sieves. Subsequent reduction of **2** with NaBH₄ provided the respective ligands. All organic compounds were characterized by ¹H/¹³C NMR, IR spectroscopy and HRMS-ESI analysis. The ¹H/¹³C NMR spectra were supportive to the proposed structures of the ligands. Finally, the target iron(II) complexes were obtained by the reaction of equimolar ligands with anhydrous FeCl₂ in DCM at room temperature. The structures of all the complexes were well determined by the IR, HRMS-ESI and elemental analysis. Further confirmation of Fe₃Me, Fe₄H, Fe₇H and Fe₁₁Me was provided in the form of single crystal X-ray structures.

In the IR spectra, the stretching vibration for the N–H bonds in complexes appeared in the range of 3193–3296 cm^{–1}, which were relatively lower in wavenumber than those observed for the free ligands (3310–3325 cm^{–1}), indicating the coordination of an sp³ nitrogen atom with iron metal.



Scheme 2 Synthesis of 2-R-6-(1-(alkylamino)methyl)pyridine ligands and their iron(II) complexes.

Single crystals of complexes **Fe3_{Me}**, **Fe4_H**, **Fe7_H** and **Fe11_{Me}** suitable for X-ray diffraction analyses were obtained by slow evaporation of their dichloromethane solution. Since the molecular structures of **Fe3_{Me}** and **Fe11_{Me}** are similar, these will therefore be discussed together.

The molecular structures of **Fe3_{Me}** and **Fe11_{Me}** are mononuclear species in which both sp^3 and sp^2 nitrogen belonging to the aminopyridine ligand serve as donor atoms. This geometry is best described as distorted tetrahedral with chloride ligands filling two other coordination sites. The molecular structure of **Fe3_{Me}** and **Fe11_{Me}** can be seen in Fig. 1 and 2 respectively. The N1–Fe1–N2 bite angles in both complexes are comparable at 80.63° for **Fe3_{Me}** and 79.91° for **Fe11_{Me}** highlighting some distortions imposed by the *N,N*-chelating ligand

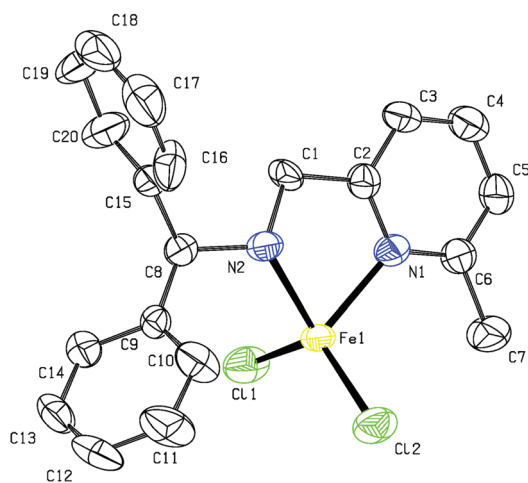


Fig. 1 Molecular structure of complex **Fe3_{Me}**: all hydrogen atoms have been omitted for clarity. Atoms are drawn at the 50% probability level. Selected bond lengths (Å) and angles (°): Fe1–N1 2.112(3), Fe1–N2 2.134(3), Fe1–Cl1 2.2190(12), Fe1–Cl2 2.2406(11), Cl1–Fe1–Cl2 123.57(5), N1–Fe1–N2 80.63(12).

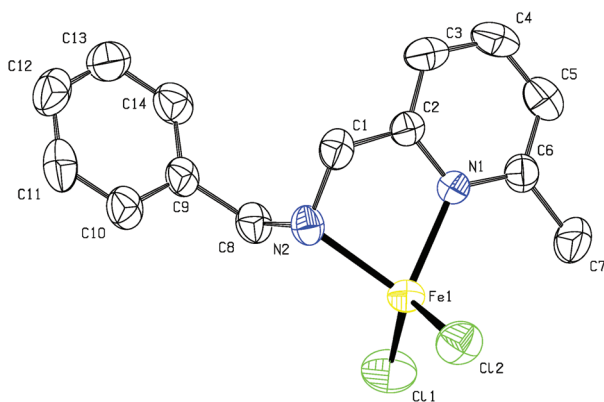


Fig. 2 Molecular structure of complex **Fe11_{Me}**: all hydrogen atoms have been omitted for clarity. Atoms are drawn at the 50% probability level. Selected bond lengths (Å) and angles (°): Fe1–N1 2.107(2), Fe1–N2 2.145(2), Fe1–Cl1 2.2241(9), Fe1–Cl2 2.2374(9), Cl1–Fe1–Cl2 120.41(4), N1–Fe1–N2 79.91(8).

on the geometry. In consequence, Cl1–Fe1–Cl2 bond angles are more open for **Fe3_{Me}** (123.57°) than **Fe11_{Me}** (120.41°). These structural features are very similar to the previously reported iron complexes.^{49,59,60} There are modest variations in the iron–nitrogen bond lengths in both iron complexes with Fe1–N2_{sp³} [2.134 Å for **Fe3_{Me}** and 2.145 Å for **Fe11_{Me}**], which are slightly longer than Fe1–N1_{sp²} [2.112 Å for **Fe3_{Me}** and 2.107 Å for **Fe11_{Me}**]. This indicates the unequal strength of coordination bonds with the metal center. Such differences in bond lengths are essentially similar to the reported iminopyridine-iron(II) complexes in which Fe–N_{imine} bond lengths are longer than Fe–N_{pyridine}.^{14,44,45}

By contrast, the molecular structure of **Fe4_H** reveals a chloride bridged centrosymmetric binuclear species as illustrated in Fig. 3. In this dimeric structure, each iron core is bound by two nitrogen atoms (sp^3 and sp^2) belonging to the aminopyridine ligand motif, one chloride per iron center bridges the iron centers. The remaining chloride serves as a monodentate ligand and each iron center adopts a distorted square pyramidal geometry. In this geometry, nitrogen (N1 and N2) and bridging chloride atoms (Cl1 and Cl1a) form the basal plane while Cl2 and Cl2a individually occupy the axial positions.

The solid state structure of **Fe7_H** is a multicore system in which each core was bridged by two chloride atoms with an Fe...Fe separation of 3.735 Å. In addition, each iron center was ligated with two nitrogen atoms (*i.e.* sp^3 and sp^2 atoms) belonging to the neutral chelating **L7_H** and four Cl atoms leading to a distorted octahedral geometry conferred to each metal center. In particular, the N_{amine} atom and one bridging chloride occupy the axial coordination site with an N2–Fe1–Cl1 angle of 170.90° reflecting non-linear behavior of the bond. While N_{pyridine} and the rest of the three chloride atoms form a basal plane of the octahedron with the iron atom lying at 0.096 Å out of the plane. It is worth mentioning that one bridging chloride atom occupies the axial position of the octahedral geometry of one metal center and is also part of the basal plane of the adjacent octahedral geometry. The plane of the chelate ring, N–C–C–N–Fe, is significantly distorted from

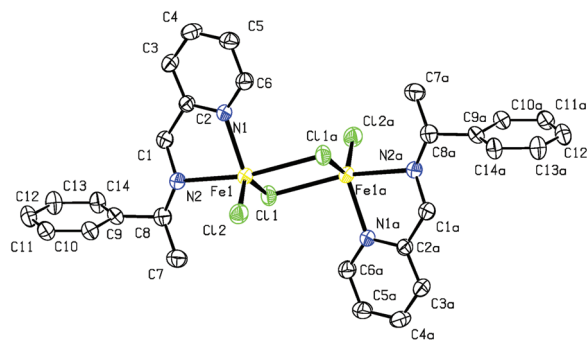


Fig. 3 Molecular structure of complex **Fe4_H**: all hydrogen atoms have been omitted for clarity. Atoms are drawn at the 30% probability level. Selected bond lengths (Å) and angles (°): Fe1–N1 2.117(2), Fe1–N2 2.245(2), Fe1–Cl1 2.3868(9), Fe1–Cl2 2.2791(9), Fe1–Cl1a 2.5668(8), Cl1–Fe1–Cl2 131.90(3), N1–Fe1–N2 77.32(8).

the plane of the pyridine ring due to the presence of the sp^3 hybridized nitrogen atom. Interestingly, the bond lengths of Fe1–Cl1 or Fe1–Cl2 are significantly shorter than those of their counterpart Fe1–Cl1a or Fe1–Cl2a [Cl1–Fe1 (2.401 Å), Cl2–Fe1 (2.438 Å), Cl1a–Fe1 (2.591 Å), Cl2a–Fe1 (2.690 Å)], indeed consistent with the previously reported *N,N*-bidentate iron complexes in which bond lengths between bridging chloride and the metal center are found to be nearly 2.400 Å (Fig. 4).^{46,60,61}

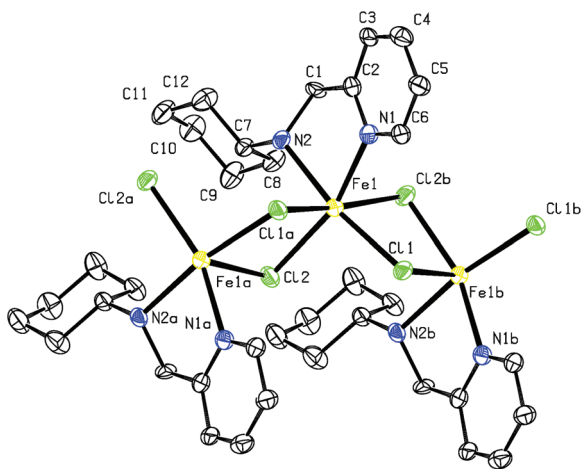


Fig. 4 Molecular structure of complex **Fe7_H**; all hydrogen atoms have been omitted for clarity. Atoms are drawn at the 30% probability level. Selected bond lengths (Å) and angles (°): Fe1–N1 2.161(8), Fe1–N2 2.252(7), Fe1–Cl1 2.401(3), Fe1–Cl2 2.438(3), Fe1–Cl1a 2.591(3), Fe1–Cl2a 2.690 (3), N1–Fe1–N2 75.4(3), Cl1–Fe1–Cl1a 94.53(10), Cl1–Fe1–Cl2a 82.80(10), Cl1a–Fe1–Cl2a 170.72(11), Cl1–Fe1–Cl2 96.55(9), Cl2–Fe1–Cl1a 84.24(8), Cl2–Fe1–Cl2a 104.83(9).

Table 1 Crystal parameters of iron complexes with different N–Fe lengths

	Fe3_{Me}	Fe4_H	Fe7_H	Fe11_{Me}	Py-imine Fe ^a
Fe–N _{pyridine}	2.112	2.107	2.117	2.161	2.103
Fe–N _{amine} /Fe–N _{imine}	2.134	2.145	2.245	2.252	2.129

^a (*E*)-2,4,4-Trimethyl-*N*-(pyridin-2-ylmethylene)pentan-2-amine iron(II) chloride.⁴⁴

As shown in Table 1, the bond distances of Fe–N(amine) and Fe–N(pyridine) are all longer than the corresponding Fe–N bond distances in Ritter's complex (CCDC 853130[†]), respectively, indicating that the donating ability of the sp^3 N-donors is lower than that of the sp^2 N-donors leading to a reduction in the electron density around the metal center. Hence, the aminopyridine-ligated iron center is more electrophilic than the iminopyridine-ligated iron center (Fe(L)²⁺). The same conclusion was drawn in palladium complexes that the α -diamine-ligated palladium center is more electrophilic than the α -diimine-ligated palladium center.⁵³

Isoprene polymerization

Screening of Fe1_H–Fe7_H with MAO. To probe the capacity of the prepared iron complexes for isoprene polymerization, MAO was used as a co-catalyst. Initially, the catalytic potential of complexes **Fe1_H–Fe7_H** was studied and the resulting polymerization data are given in Table 2. The observed catalytic activities of these catalysts appended with different substituents varied in the order **Fe5_H** [CH₂Ph] = **Fe6_H** [CHMe₂] = **Fe7_H** [C₆H₁₁] > **Fe4_H** [CHMePh] > **Fe2_H** [CHPh₂] > **Fe1_H** [CPh₃] > **Fe3_{Me}** [CHPh₂]. This decreasing trend of activity clearly showed that steric factors are influential and the catalysts bearing the least steric bulky group tended to give higher activities. The complexes **Fe5_H** [CH₂Ph] = **Fe6_H** [CHMe₂] = **Fe7_H** [C₆H₁₁] bearing less sterically hindered groups exhibited standout performance in terms of activity as high as 6.8×10^4 g mol^{−1} h^{−1} with >99% conversion (Table 2, entries 5–7). This activity dramatically reduced to 4.7×10^4 g mol^{−1} h^{−1} when relatively more bulky groups were installed in the catalysts (Table 2, entry 4). The lower activity of 2.3×10^4 g mol^{−1} h^{−1} was observed when a triphenyl group was attached to the *N*-alkyl unit (Table 2, entry 1). This decreasing trend of activities as a function of steric hindrance suggests that more bulky groups occupying the space around the metal center in the active species slow down the rate of coordination and insertion of the monomer, thus lower activity was observed.^{23–25} As part of our continuous efforts to examine the steric effect, a methyl group was installed at the *ortho* position of pyridine and its effect on the polymerization of isoprene was studied. Introduction of a

Table 2 Fe1_H–Fe7_H/MAO promoted isoprene polymerization^a

Entry	Cat.	Yield%	Activity ^b	Microstructure ^c (%)			<i>M_n</i> ^d (× 10 ⁴)	PDI ^d
				<i>cis</i> -1,4	<i>trans</i> -1,4	3,4		
1	Fe1_H	33	2.3	53	0	47	11.2	1.7
2	Fe2_H	68	4.7	9	69	22	2.0	3.7
3	Fe3_{Me}	13	0.8	69	4	27	12.3	1.6
4	Fe4_H	70	4.7	46	8	46	0.2	1.6
5	Fe5_H	>99	6.8	29	22	49	2.6	4.7
6	Fe6_H	>99	6.8	41	10	49	3.9	3.9
7	Fe7_H	>99	6.8	44	4	52	8.1	2.1
							11.1	1.7

^a Polymerization conditions: solvent: 5 mL toluene; complex: 10 μmol; isoprene: 20 mmol; time: 2 h; *T*: 25 °C; MAO/Fe: 500. ^b 10⁴ g mol^{−1} h^{−1}. ^c Determined by ¹H NMR and ¹³C NMR. ^d Determined by gel permeation chromatography (GPC).

methyl group on the *ortho* position of the pyridine moiety exhibited a negative effect on the catalytic activity as Fe3_{Me} [CHPh_2] displayed the lowest activity of $0.8 \times 10^4 \text{ g mol}^{-1} \text{ h}^{-1}$ with only 13% conversion (Table 2, entry 3). Interestingly, introducing a bulky group near the active species favored the enhancement of the molecular weight of the resultant polymer. For instance, Fe3_{Me} [CHPh_2] bearing a methyl group at the sixth position of pyridine afforded polyisoprene with the highest molecular weight up to 12.3×10^4 and Fe1_{H} bearing a bulky CPh_3 substituent produced polyisoprene with a comparable molecular weight (11.2×10^4). It is assumed that bulky groups protect the active species which would not only align the coordination and insertion of a monomer but also promote the chain propagation as compared to the chain transfer to the aluminum species.^{62,63} The molecular weight distributions (PDI) of the obtained polymers varied from narrow to moderately broad and were bimodal as can be seen in Fig. S49.†

The microstructural properties of the obtained polyisoprene have been determined by ^1H and ^{13}C NMR spectroscopy (recorded in deuterated chloroform at room temperature) and confirmed by the characteristic peaks listed in the literature.^{64,65} According to the characteristic peaks that appeared in the ^1H and ^{13}C NMR spectra, in general, most of the obtained polyisoprene possessed nearly an equal amount of *cis*-1,4 and 3,4 units (Table 2 & Fig. 5). For example, the polymer obtained by complex Fe4_{H} [CHMePh] equally favors *cis*-1,4 (46%) and 3,4 (46%) monomer insertion. Interestingly, Fe2_{H} [CHPh_2] and Fe3_{Me} [CHPh_2] catalyzed isoprene polymerization showed essentially different selectivity of monomer insertion: the Fe2_{H} [CHPh_2] based polymer was composed of 69% *trans*-1,4 units, while 69% *cis*-1,4 monomer insertion was observed in the case of Fe3_{Me} [CHPh_2] promoted polymerization (Fig. 6 & 7). These polymerization results indicated that how fine tuning of the ligand structure gives different microstructures of the polymer.

Screening of the reaction conditions using Fe5_{H} /MAO. In order to ascertain the effects of reaction parameters such as

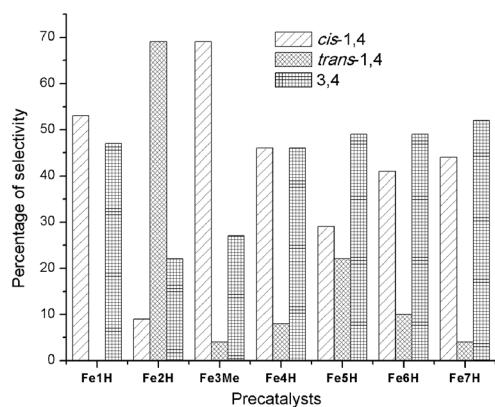


Fig. 5 Microstructural properties of polyisoprene obtained by Fe1_{H} – Fe7_{H} /MAO (Table 2, entries 1–7).

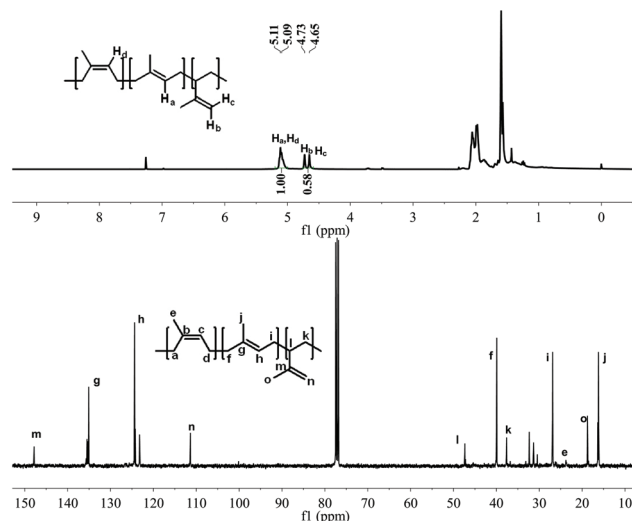


Fig. 6 ^1H and ^{13}C NMR spectra of the representative sample of polyisoprene obtained by Fe2_{H} /MAO (Table 2, entry 2).

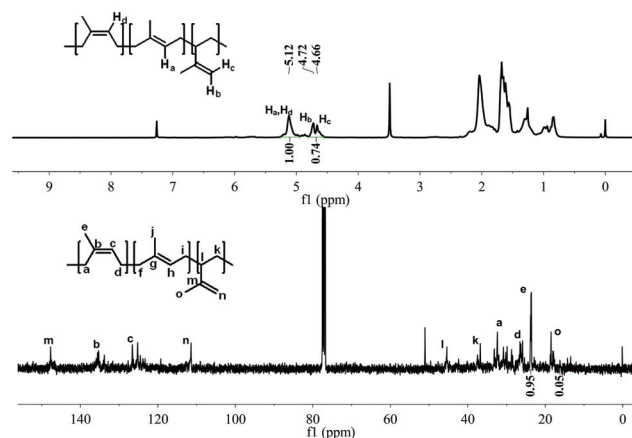


Fig. 7 ^1H and ^{13}C NMR spectra of the representative sample of polyisoprene obtained by Fe3_{Me} /MAO (Table 2, entry 3).

Al/Fe ratio, IP/Fe ratio and reaction temperature on isoprene polymerization, Fe5_{H} was used as a test precatalyst in combination with the MAO cocatalyst and the resulting polymerization data are summarized in Table 3. Firstly, temperature was fixed at 25 °C, and the Al/Fe ratio consistently decreased from 500 to 200 (Table 3, entries 1–3), resulting in 500 being identified as the best Al/Fe ratio with the catalytic activity of Fe5_{H} /MAO reaching a peak in activity of $81.6 \times 10^4 \text{ g mol}^{-1} \text{ h}^{-1}$ with >99% conversion (Table 3, entry 1). On decreasing the Al/Fe ratio to 200, activity as well as conversion consistently reduced to $62.4 \times 10^4 \text{ g mol}^{-1} \text{ h}^{-1}$ with a conversion of 77% (Table 3, entry 3). Nevertheless, this polyisoprene revealed no change in the selectivity of monomer insertion on decreasing the Al/Fe ratio. Changes in the Al/Fe ratio showed no regular influence on the molecular weight and PDI of the resultant polymer. On increasing the IP/Fe ratio from 2000 to 10 000, nonetheless the conversion of the monomer reduced to 47% but the activity

Table 3 Screening of the reaction conditions using Fe5_H/MAO and Fe8_H–Fe11_{Me}/MAO promoted isoprene polymerization^a

Entry	Cat.	Al/Fe	IP/Fe	T/°C	Yield %	Activity ^d	Microstructure ^e (%)			M _n ^f (× 10 ⁴)	PDI ^f
							<i>cis</i> -1,4	<i>trans</i> -1,4	3,4		
1	Fe5 _H	500	2000	25	>99	81.6	29	23	48	4.1	4.0
2	Fe5 _H	300	2000	25	87	70.8	28	25	47	4.8	4.2
3	Fe5 _H	200	2000	25	77	62.4	28	25	47	4.5	4.0
4	Fe5 _H	500	10 000	25	47	190.6	29	17	54	6.0	2.4
5	Fe5 _H	500	2000	50	71	58.0	32	20	48	3.8	7.3
6 ^b	Fe5 _H	500	2000	−40	67	9.1	43	7	50	8.3	2.7
7 ^c	Fe5 _H	500	2000	−78	Trace	—	—	—	—	—	—
8	Fe8 _H	200	2000	25	65	53.4	18	38	44	4.1	3.2
9	Fe9 _H	200	2000	25	91	74.4	32	19	49	5.2	4.1
10	Fe10 _H	200	2000	25	70	56.7	36	17	47	3.7	5.2
11 ^c	Fe11 _{Me}	200	2000	25	11	0.7	44	15	41	6.3	3.2

^a Polymerization conditions: solvent: 5 mL toluene; complex: 10 μmol; time: 10 min. ^b 1 h. ^c 2 h. ^d 10⁴ g mol^{−1} h^{−1}. ^e Determined by ¹H NMR and ¹³C NMR. ^f Determined by gel permeation chromatography (GPC).

dramatically improved to 190.6 × 10⁴ g mol^{−1} h^{−1} over a run time of 10 min (Table 3, entry 4). With the Al/Fe and IP/Fe ratios fixed at 500 and 2000 respectively, reaction temperatures were varied between 50 °C and −78 °C (Table 3, entries 1 & 5–7). According to the data in Table 3, a peak in activity of 81.6 × 10⁴ g mol^{−1} h^{−1} was observed at 25 °C (Table 3, entry 1), while a higher temperature of 50 °C led to a decrease in activity (Table 3, entry 5) reflecting lower thermal stability of the prepared iron complexes. It can be ascribed to the less coordinating ability of the amine moiety than the imine moiety. Indeed similar observations were found for iron-catalyzed olefin polymerization.^{24,25} Polymerization tests performed at −40 °C and −78 °C also resulted in lower activities, indeed a trace amount of polymer was observed at −78 °C. This drop in activity can be attributed to the lower activation process of iron species at such a lower temperature. Expectedly, the molecular weight of polymers gradually decreased on elevating the reaction temperature (Fig. 8). It can be ascribed to an increased rate of chain transfer reaction and termination as compared to the chain propagation at higher temperatures.^{24,25} Regarding the microstructural properties of the polymers prepared at different temperatures, it was

observed that higher temperatures showed no notable effect on the selectivity of monomer insertion, however, a decrease in the reaction temperature led to an improvement in the *cis*-1,4 selectivity from 29% to 43% at 25 °C and −40 °C respectively. Meanwhile, *trans*-1,4 selectivity consistently reduced and no substantial change in the 3,4 selectivity was observed on elevating the reaction temperature.

Screening of Fe8_H–Fe11_{Me} with MAO. In order to establish a relationship between structural variations in the precatalysts and their catalytic performance, the remaining four precatalysts, Fe8_H [R¹ = H; R² = OMe], Fe9_H [R¹ = H; R² = CF₃], Fe10_H [R¹ = Me; R² = Me], and Fe11_{Me} [R¹ = H; R² = H] were also employed for isoprene polymerization (Table 3, entries 8–11). Typical polymerization tests were performed in 5 mL toluene with an IP/Fe ratio of 2000 at 25 °C over a run time of 10 minutes. When the polymerization tests were performed with Fe8_H–Fe10_H, quantitative conversions were obtained with the Al/Fe ratio fixed at 500 (ESI† section 1). For comparing the activities of different catalysts, the Al/Fe ratio decreased to 200. The overall activity was decreased in the order of Fe9_H [R¹ = H; R² = CF₃] > Fe5_H [R¹ = H; R² = H] > Fe10_H [R¹ = Me; R² = Me] > Fe8_H [R¹ = H; R² = OMe] > Fe11_{Me} [R¹ = H; R² = H]. After careful examination of the polymerization results, it was found that catalytic activities gradually increased with respect to the electron-withdrawing nature of the *para* substituents: Fe9_H [R¹ = H; R² = CF₃] was found as the standout performer exhibiting the highest activity of 74.4 × 10⁴ g mol^{−1} h^{−1} with 91% conversion (Table 3, entry 9). By contrast, Fe8_H [R¹ = H; R² = OMe] bearing an electron-donating group (*i.e.* OMe) showed a negative impact on the activity (Table 3, entry 8). Similar to the findings described above (Table 3, entry 3), the introduction of the methyl group at the sixth position of pyridine again showed a negative effect on the catalytic performance as it led to a lower activity of 0.7 × 10⁴ g mol^{−1} h^{−1} with 11% conversion (Table 3, entry 11), suggesting that the methyl group covers more space around the active species which in turn reduces the insertion and coordination of the monomer or in part, due to the interaction of hydrogen of this methyl group with the

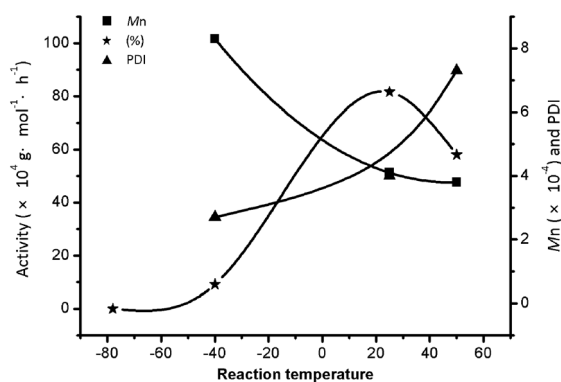


Fig. 8 Changes in the conversion (%), M_n and PDI of polyisoprene obtained at different reaction temperatures (Table 3, entries 1 and 5–7).

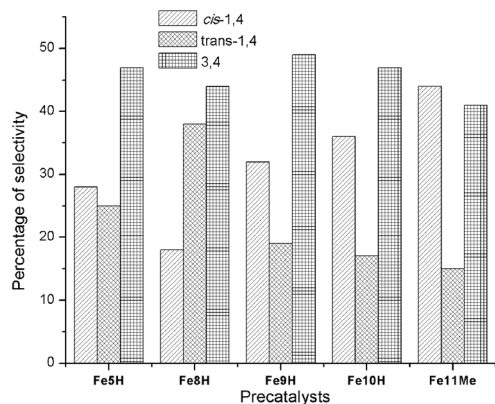


Fig. 9 Microstructural properties of polyisoprene obtained by Fe5_H , Fe8_H – Fe11_Me /MAO (Table 3, entries 3 and 8–11).

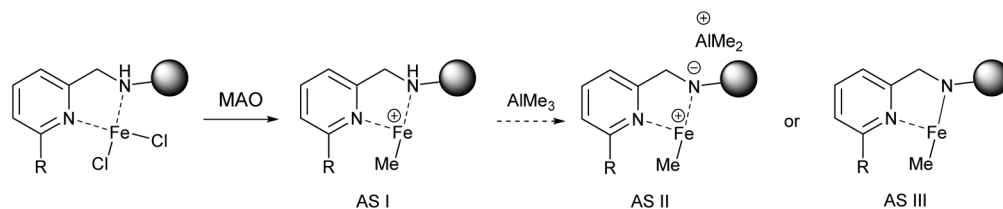
active metal center.^{23–25} Regarding the properties of the polymer, the molecular weights fall in the range of 3.7 – 6.3×10^4 and a more sterically hindered precatalyst produced polyisoprene with a relatively higher molecular weight. This fact is not ambiguous, indeed consistent with the literature.^{23–25} In addition, broad and bimodal molecular weight distributions are the characteristics of the resultant polymer. Regarding the microstructural properties of the resultant polymer, from a general point of view, 3,4 unit enriched polymers were observed in all cases with the value of about 50% (Fig. 9). According to what has been previously reported, the polyisoprene catalyzed by iminopyridine-iron catalysts possessed a high content of 1,4 motif with only about 20% content of 3,4 motif.^{44,45} Besides, comparatively more sterically hindered precatalysts favored *cis*-1,4 enchainment rather than *trans*-1,4. For instance, the Fe11_Me based polymer bearing a methyl group at the sixth position showed high selectivity of *cis*-1,4 monomer insertion which is higher in comparison with the value of 29% observed in the Fe5_H based polymer.

Mechanistic investigation of enriched 3,4-polyisoprene by aminopyridine-iron complexes

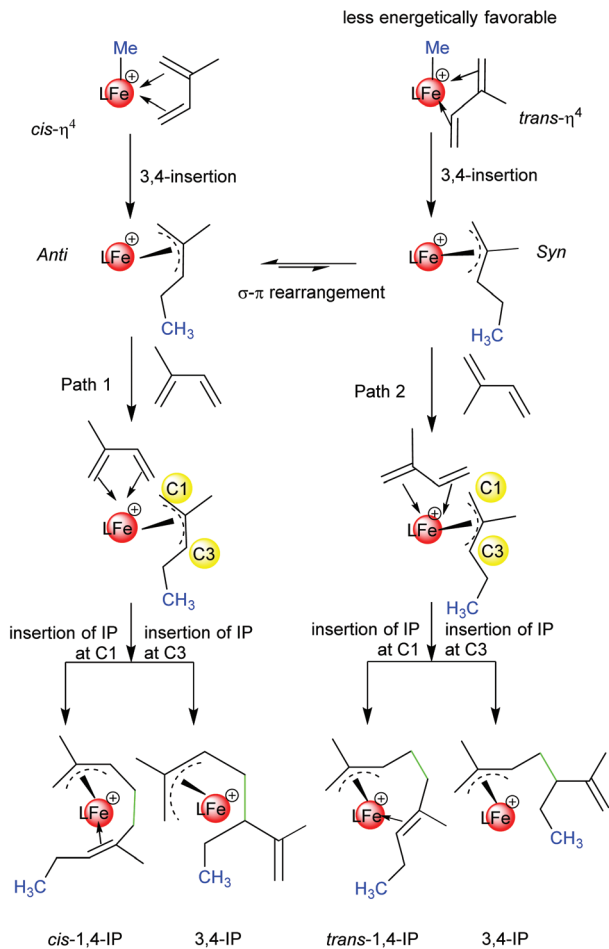
In general, the deprotonation of the amine group by a strong base, such as *n*BuLi, is feasible. The production of the amide group can react with the metal to generate an amide–metal combination model.⁵⁴ Meanwhile, we have proved that the L2_H ligand can be deprotonated by excess AlMe_3 through ^1H NMR in C_6D_6 (ESI Fig. S51[†]). Therefore, a crucial problem with

regard to the active species involved in the polymerization needs to be addressed, whether it is cation pyridine-amine (AS I), cation pyridine-amide (AS II) or neutral pyridine-amide (AS III) active species on activation with MAO co-catalysts (Scheme 3). For this confirmation, we synthesized the pyridine-amide iron complex with an identical substituent to the Fe2_H obtained by the reaction of anhydrous FeCl_2 with an ionic ligand which was deprotonated by *n*-butyllithium base (see the details of complex synthesis in ESI,† section 2). Later, the catalytic potential of Fe12_H for isoprene polymerization was studied under similar conditions to those used for Fe2_H based polymerization. The polymerization results exhibited activity up to $6.8 \times 10^4 \text{ g mol}^{-1} \text{ h}^{-1}$ (full conversion) with a 1/1 ratio of *cis*-1,4 and 3,4 units, which is essentially different from the selectivity observed for the Fe2_H promoted polymerization. This comparison precluded the involvement of active species (AS III) in the polymerization performed using the Fe2_H catalyst. Our conclusion was also supported by ethylene polymerization using quinolinolato-amine titanium complexes by Jin⁶⁶ and pyridine-amine nickel complexes by Wu.⁵⁵ Therefore, we proposed the active structure of the pyridine-amine Fe complexes as AS I, while the deprotonation of the catalyst by AlMe_3 as AS II can't be ruled out. Probably, the active species AS I and AS II could co-exist and were involved in polymerization.

Furthermore, the title aminopyridine-iron catalysts resulted in different microstructures of polyisoprene from those of the previously reported iminopyridine-iron chloride catalyzed isoprene polymerization, indicating a different activation process which results in different regioselectivity. For iron complexes with bidentate nitrogen ligands, the crystal analysis showed that the bond distances of $\text{Fe-N}_{\text{amine}}$ are longer than the $\text{Fe-N}_{\text{imine}}$ bond distances, indicating that the electron donating ability of the sp^3 N-donors is lower than that of the sp^2 N-donors, which leads to the lower electron density around the metal center. Hence, the aminopyridine-ligated iron center is more electrophilic than the iminopyridine-ligated iron center (Fe(L)^{2+}). Such changes affect the binding interaction between the metal and the coordination donor as well as the opening environment near the metal center. Based on this, the isoprene monomer would coordinate to the iron atom through the η^4 bond including *cis*- η^4 or *trans*- η^4 rather than the η^2 bond as shown in Scheme 4. The insertion of the coordinated monomer leads to the formation of *anti*- η^3 or *syn*- η^3 allyl-Fe intermediates, respectively. The allylic unit has two reactive sites, C1 and C3. The 1,4 unit is formed by insertion of the



Scheme 3 Possible active species during the polymerization.



Scheme 4 Possible mode of formation of polyisoprene.

incoming monomer at C1, while a 3,4 unit is formed by insertion of the incoming monomer at C3. In the case of $\text{Fe}5_{\text{H}}$ mediated polymerization, the $\text{cis-}\eta^4$ type of coordination-insertion of monomer was expected as 3,4 unit enriched polyisoprene was obtained. Similar findings have been reported in rare earth and cobalt systems.^{67,68}

Conclusions

In conclusion, novel iron(II) complexes based on aminopyridine ligands were synthesized and well characterized. The molecular structures of complexes $\text{Fe}3_{\text{Me}}$, $\text{Fe}4_{\text{H}}$, $\text{Fe}7_{\text{H}}$ and $\text{Fe}11_{\text{Me}}$ were characterized by single crystal X-ray diffraction in the solid state. All complexes displayed two combination fashions (pyridine (sp^2) and amine (sp^3)) leading to a distinctive effect on isoprene polymerization. Upon activation with a MAO cocatalyst, all catalysts showed moderate to high activities with a maximum value of $190.6 \times 10^4 \text{ g mol}^{-1} \text{ h}^{-1}$ obtained by $\text{Fe}5_{\text{H}}[\text{CH}_2\text{Ph}]$ toward isoprene polymerization. Introduction of substituents on the amine moiety and to the *ortho*-position of pyridine exhibited a notable effect on the activity, meanwhile monomer enchainment favored in the 3,4 unit. The molecular

weight of polymers can be controlled in the range from 2.0×10^4 to 11.2×10^4 with narrow to broad molecular weight distributions in the range of 1.7–7.3. Possible mechanistic consideration of enriched 3,4-polyisoprene catalyzed by aminopyridine-iron(II) complexes was provided.

Experimental

General procedures

All manipulations of air and/or moisture sensitive compounds were performed using standard Schlenk techniques. Toluene, dichloromethane (DCM), tetrahydrofuran (THF) and hexane were purchased from Sinopharm Chemical Reagent, dried over sodium benzophenone ketyl (toluene, THF) or calcium hydride (DCM, hexane) and distilled under an argon atmosphere prior to use. ^1H and ^{13}C NMR spectra were recorded on a Bruker Avance III 400 MHz spectrometer using CDCl_3 as the solvent and trimethylsilane (TMS) as the internal reference. Chemical shifts and coupling constants were given in ppm and in Hz respectively. Attenuated total reflection-infrared (ATR-IR) spectroscopy was performed using a Thermo Scientific Nicolet iN10. The Greek alphabet ' ν ' stands for the stretching vibration wavenumber. Elemental analysis was carried out on a Vario EL III elemental analyzer at the Shanghai Institute of Organic Chemistry, Chinese Academy of Sciences. Mass spectra for new organic compounds were recorded using a maXis II of Bruker Daltonics Corporation, while for Fe(II) complexes, the mass spectra were recorded using an ACQUITY™ UPLC & Q-TOF MS Premier at the Analytical Center of Shanghai Jiao Tong University. X-ray diffraction data were collected on a Smart 1000 diffractometer with a Mo-K α X-ray source ($\lambda = 0.71073 \text{ \AA}$) or Cu-K α radiation ($\lambda = 1.54178 \text{ \AA}$). Molecular weights and polydispersity indices (PDI) of polyisoprene were measured by high temperature gel permeation chromatography (HGPC, PL-GPC 220, Agilent Technologies) using trichlorobenzene as the eluent and polystyrenes as standards. Isoprene was purchased from Aladdin Industrial Corporation, dried over CaH_2 and distilled prior to use. The MAO which was purchased from Aike Reagent contains 10% AlMe_3 and was used without further purification. All other reagents were purchased from commercial sources and used without further purification.

Synthesis of ligands

2-(1-(Triphenylmethylamino)methyl)pyridine, $\text{L}1_{\text{H}}$. $\text{L}1_{\text{H}}$ was prepared using a two-step procedure.⁶⁹ In the first step, triphenylmethylamine (2.74 g, 10.55 mmol) and activated 4 Å molecular sieves (2.00 g) were added into the solution of 2-pyridinecarboxaldehyde (1.13 g, 10.55 mmol) in dry DCM (20.0 mL) and stirred at room temperature. After overnight stirring, all the volatiles were evaporated under reduced pressure and the crude product was washed twice with cold methanol affording an orange solid (3.10 g, 84% yield). In the second step,⁷⁰ the resulting imine (0.52 g, 1.49 mmol) was dissolved in methanol, and NaBH_4 (0.57 g, 15.00 mmol) was added. The solution was stirred overnight. The product was extracted by

DCM. The organic layer was dried over MgSO_4 and filtered. The solvent was evaporated under reduced pressure to give the crude product as a white solid, which was further purified by silica gel column chromatography (0.32 g, 61% yield). ^1H NMR (400 MHz, CDCl_3 , 298 K): δ 8.49 (ddd, $J = 4.8, 1.8, 0.8$ Hz, 1H), 7.64 (td, $J = 7.8, 1.8$ Hz, 1H), 7.58–7.51 (m, 6H), 7.46 (d, $J = 7.8$ Hz, 1H), 7.31–7.24 (m, 6H), 7.21–7.16 (m, 3H), 7.12 (ddd, $J = 7.6, 4.8, 1.2$ Hz, 1H), 3.52 (s, 2H), 2.59 (s, 1H). ^{13}C NMR (100 MHz, CDCl_3 , 298 K): δ 160.5, 149.2, 146.1, 136.6, 128.8, 128.0, 126.5, 122.0, 121.8, 71.2, 49.7. FTIR (KBr, cm^{-1}): 3313 (ν (N–H)), 3054, 2923, 1956, 1592, 1569, 1428, 1354, 1109, 1031, 773, 708. HRMS-ESI (m/z): $[\text{M} + \text{H}]^+$ calcd for $\text{C}_{25}\text{H}_{23}\text{N}_2$, 351.1861; found, 351.1854.

2-(1-(Diphenylmethylamino)methyl)pyridine, L2_H. Using the similar procedure established for the synthesis of L1_H, L2_H was obtained as a pale yellow solid. 88% (2.54 g) and 74% (1.51 g) yield was obtained in the first and second step, respectively. ^1H NMR (400 MHz, CDCl_3 , 298 K): δ 8.54 (ddd, $J = 4.8, 1.8, 1.0$ Hz, 1H), 7.61 (td, $J = 7.6, 1.8$ Hz, 1H), 7.47–7.40 (m, 4H), 7.33–7.25 (m, 5H), 7.23–7.17 (m, 2H), 7.14 (ddd, $J = 7.6, 4.8, 1.2$ Hz, 1H), 4.87 (s, 1H), 3.87 (s, 2H), 2.52 (s, 1H). ^{13}C NMR (100 MHz, CDCl_3 , 298 K): δ 159.8, 149.4, 143.9, 136.4, 128.6, 127.5, 127.1, 122.6, 122.0, 77.5, 53.5. FTIR (KBr, cm^{-1}): 3325 (ν (N–H)), 3044, 2818, 1958, 1591, 1566, 1450, 1342, 1149, 993, 743, 704. HRMS-ESI (m/z): $[\text{M} + \text{H}]^+$ calcd for $\text{C}_{19}\text{H}_{19}\text{N}_2$, 275.1548; found, 275.1546.

2-Methyl-6-(1-(diphenylmethylamino)methyl)pyridine, L3_{Me}. Using the similar procedure established for the synthesis of L1_H, L3_H was obtained as a pale yellow solid. 68% (1.10 g) and 99% (1.00 g) yield was obtained in the first and second step, respectively. ^1H NMR (400 MHz, CDCl_3 , 298 K): δ 7.52 (s, 1H), 7.48–7.42 (m, 4H), 7.30 (t, $J = 7.6$ Hz, 4H), 7.22 (d, $J = 7.4$ Hz, 2H), 7.08 (d, $J = 7.6$ Hz, 1H), 7.01 (d, $J = 7.6$ Hz, 1H), 4.88 (s, 1H), 3.83 (s, 2H), 2.53 (s, 3H). ^{13}C NMR (100 MHz, CDCl_3 , 298 K): δ 159.1, 158.1, 144.1, 136.7, 128.6, 127.6, 127.1, 121.5, 119.4, 77.5, 77.2, 76.8, 67.2, 53.6, 24.6. FTIR (KBr, cm^{-1}): 3319 (ν (N–H)), 3060, 3025, 2921, 2829, 1953, 1593, 1577, 1492, 1452, 1342, 1117, 1028, 753, 702. HRMS-ESI (m/z): $[\text{M} + \text{H}]^+$ calcd for $\text{C}_{20}\text{H}_{21}\text{N}_2$, 289.1705; found, 289.1701.

2-(1-(1-Phenylethylamino)methyl)pyridine, L4_H. Using the similar procedure established for the synthesis of L1_H, L4_H was obtained as a pale yellow solid. 92% (2.00 g) and 80% (0.67 g) yield was obtained in the first and second step, respectively. ^1H NMR (400 MHz, CDCl_3 , 298 K): δ 8.55 (d, $J = 4.8$ Hz, 1H), 7.60 (td, $J = 7.8, 1.8$ Hz, 1H), 7.40–7.30 (m, 4H), 7.26–7.22 (m, 1H), 7.20 (d, $J = 7.8$ Hz, 1H), 7.14 (ddd, $J = 7.6, 4.8, 1.2$ Hz, 1H), 3.83 (q, $J = 6.6$ Hz, 1H), 3.75 (s, 2H), 2.19 (s, 1H), 1.42 (d, $J = 6.6$ Hz, 3H). ^{13}C NMR (100 MHz, CDCl_3 , 298 K): δ 159.9, 149.4, 145.5, 136.5, 128.6, 127.1, 126.9, 122.6, 122.0, 58.2, 53.2, 24.6. FTIR (KBr, cm^{-1}): 3317 (ν (N–H)), 3066, 2964, 2925, 1950, 1591, 1450, 1433, 1369, 1128, 994, 761, 701. HRMS-ESI (m/z): $[\text{M} + \text{H}]^+$ calcd for $\text{C}_{14}\text{H}_{17}\text{N}_2$, 213.1392; found, 213.1387.

2-(1-(Phenylmethylamino)methyl)pyridine, L5_H. Using the similar procedure established for the synthesis of L1_H, L5_H was obtained as a pale yellow solid. 68% (2.5 g) and 62%

(1.01 g) yield was obtained in the first and second step, respectively. ^1H NMR (400 MHz, CDCl_3 , 298 K): δ 8.61–8.52 (m, 1H), 7.63 (td, $J = 7.8, 1.8$ Hz, 1H), 7.39–7.29 (m, 5H), 7.24 (d, $J = 6.8$ Hz, 1H), 7.18–7.13 (m, 1H), 3.93 (s, 2H), 3.84 (s, 2H), 2.19 (s, 1H). ^{13}C NMR (100 MHz, CDCl_3 , 298 K): δ 159.9, 149.4, 140.2, 136.5, 128.5, 128.4, 127.1, 122.4, 122.0, 54.6, 53.6. FTIR (KBr, cm^{-1}): 3313 (ν (N–H)), 3061, 3027, 2920, 2838, 1952, 1591, 1454, 1433, 1362, 1120, 994, 753, 699. HRMS-ESI (m/z): $[\text{M} + \text{H}]^+$ calcd for $\text{C}_{14}\text{H}_{17}\text{N}_2$, 199.1235; found, 199.1231.

2-(1-(1-Methylethylamino)methyl)pyridine, L6_H. Using the similar procedure established for the synthesis of L1_H, L6_H was obtained as a pale yellow solid. 92% (4.07 g) and 66% (1.34 g) yield was obtained in the first and second step, respectively. ^1H NMR (400 MHz, CDCl_3 , 298 K): δ 8.55 (ddd, $J = 5.0, 1.8, 1.0$ Hz, 1H), 7.70 (td, $J = 7.8, 1.8$ Hz, 1H), 7.60 (dt, $J = 7.8, 1.2$ Hz, 1H), 7.23 (ddd, $J = 7.6, 4.8, 1.2$ Hz, 1H), 4.20 (s, 2H), 3.21 (hept, $J = 6.6$ Hz, 1H), 1.36 (d, $J = 6.6$ Hz, 6H). ^{13}C NMR (100 MHz, CDCl_3 , 298 K): δ 153.4, 149.4, 137.3, 123.8, 123.4, 49.5, 49.5, 20.3. FTIR (KBr, cm^{-1}): 3312 (ν (N–H)), 2964, 2926, 2854, 1592, 1570, 1473, 1434, 1174, 995, 756. HRMS-ESI (m/z): $[\text{M} + \text{H}]^+$ calcd for $\text{C}_9\text{H}_{15}\text{N}_2$, 151.1235; found, 151.1230.

2-(1-(Cyclohexylamino)methyl)pyridine, L7_H. Using the similar procedure established for the synthesis of L1_H, L7_H was obtained as a pale yellow solid. 93% (5.70 g) and 94% (1.78 g) yield was obtained in the first and second step, respectively. ^1H NMR (400 MHz, CDCl_3 , 298 K): δ 8.54 (dt, $J = 4.8, 1.2$ Hz, 1H), 7.63 (td, $J = 7.6, 1.8$ Hz, 1H), 7.32–7.28 (m, 1H), 7.14 (ddd, $J = 7.4, 4.8, 1.2$ Hz, 1H), 3.93 (s, 2H), 2.54–2.44 (m, 1H), 2.15 (s, 1H), 1.924 (ddt, $J = 9.8, 3.8, 1.8$ Hz, 2H), 1.74 (dt, $J = 12.2, 3.6$ Hz, 2H), 1.65–1.57 (m, 1H), 1.31–1.09 (m, 5H). ^{13}C NMR (100 MHz, CDCl_3 , 298 K): δ 160.2, 149.3, 136.5, 122.4, 121.9, 56.7, 52.5, 33.6, 26.2, 25.1. FTIR (KBr, cm^{-1}): 3310 (ν (N–H)), 3065, 3009, 2926, 2852, 1592, 1570, 1433, 1371, 1126, 1048, 755. HRMS-ESI (m/z): $[\text{M} + \text{H}]^+$ calcd for $\text{C}_{13}\text{H}_{18}\text{N}_2$, 191.1548; found, 191.2980.

2-(1-(4-Methoxyphenylmethylamino)methyl)pyridine, L8_H. Using the similar procedure established for the synthesis of L1_H, L8_H was obtained as a pale yellow solid. 73% (3.10 g) and 91% (0.31 g) yield was obtained in the first and second step, respectively. ^1H NMR (400 MHz, CDCl_3 , 298 K): δ 8.59–8.51 (m, 1H), 7.64 (tt, $J = 7.6, 1.8$ Hz, 1H), 7.35–7.19 (m, 3H), 7.15 (ddd, $J = 7.6, 4.8, 1.2$ Hz, 1H), 6.92–6.81 (m, 2H), 3.91 (s, 2H), 3.79 (s, 3H), 3.78 (s, 2H), 2.14 (s, 1H). ^{13}C NMR (100 MHz, CDCl_3 , 298 K): δ 159.9, 158.8, 149.4, 136.5, 132.4, 129.6, 122.5, 122.0, 113.9, 55.4, 54.6, 53.0. FTIR (KBr, cm^{-1}): 3312 (ν (N–H)), 3007, 2934, 2835, 2058, 1884, 1611, 1510, 1301, 1247, 1176, 1034, 816, 758. HRMS-ESI (m/z): $[\text{M} + \text{H}]^+$ calcd for $\text{C}_{14}\text{H}_{17}\text{N}_2\text{O}$, 229.1341; found, 229.1335.

2-(1-(4-Trifluoromethylphenylmethylamino)methyl)pyridine, L9_H. Using the similar procedure established for the synthesis of L1_H, L9_H was obtained as a pale yellow solid. 79% (3.9 g) and 93% (0.93 g) yield was obtained in the first and second step respectively. ^1H NMR (400 MHz, CDCl_3 , 298 K): δ 8.57 (dt, $J = 5.0, 1.4$ Hz, 1H), 7.64 (td, $J = 7.6, 1.8$ Hz, 1H), 7.58 (d, $J = 8.0$ Hz, 2H), 7.49 (d, $J = 8.0$ Hz, 2H), 7.29 (d, $J = 7.8$ Hz, 1H), 7.17 (m, $J = 7.6, 4.8, 1.2$ Hz, 1H), 3.92 (s, 2H), 3.91 (s, 2H), 2.13 (s,

1H). ^{19}F NMR (376 MHz, CDCl_3 , 298 K): δ -62.39. ^{13}C NMR (100 MHz, CDCl_3 , 298 K): δ 159.5, 149.5, 144.4, 136.6, 129.4 (q, $J = 32.2$ Hz), 128.5, 125.4 (q, $J = 3.8$ Hz), 124.4 (q, $J = 273.0$ Hz), 122.5, 122.2, 54.6, 53.1. FTIR (KBr, cm^{-1}): 3313 (ν (N-H)), 3068, 3013, 2924, 2839, 1922, 1592, 1434, 1327, 1162, 1123, 1066, 818, 757. HRMS-ESI (m/z): $[\text{M} + \text{H}]^+$ calcd for $\text{C}_{14}\text{H}_{14}\text{F}_3\text{N}_2$, 267.1109; found, 267.1103.

2-(1-(2,4,6-Trimethylphenylmethylamino)methyl)pyridine, L10_H. Using the similar procedure established for the synthesis of **L1_H**, **L4_H** was obtained as a pale yellow solid. 89% (4.0 g) and 69% (0.64 g) yield was obtained in the first and second step respectively. ^1H NMR (400 MHz, CDCl_3 , 298 K): δ 8.59–8.53 (m, 1H), 7.65 (td, $J = 7.6$, 1.8 Hz, 1H), 7.38 (d, $J = 7.8$ Hz, 1H), 7.19–7.12 (m, 1H), 6.83 (s, 2H), 3.99 (s, 2H), 3.77 (s, 2H), 2.33 (s, 6H), 2.24 (s, 3H). ^{13}C NMR (100 MHz, CDCl_3 , 298 K): δ 160.3, 149.3, 137.2, 136.6, 136.5, 133.6, 129.1, 122.5, 122.0, 55.6, 47.3, 21.0, 19.6. FTIR (KBr, cm^{-1}): 3323 (ν (N-H)), 3006, 2916, 2860, 2388, 1590, 1570, 1433, 1375, 1094, 1047, 850, 756. HRMS-ESI (m/z): $[\text{M} + \text{H}]^+$ calcd for $\text{C}_{16}\text{H}_{21}\text{N}_2$, 241.1705; found, 241.1700.

2-Methyl-6-(1-(phenylmethylamino)methyl)pyridine, L11_H. Using the similar procedure established for the synthesis of **L1_H**, **L4_H** was obtained as a pale yellow solid. 69% (2.4 g) and 88% (0.44 g) yield was obtained in the first and second step respectively. ^1H NMR (400 MHz, CDCl_3 , 298 K): δ 7.52 (t, $J = 7.6$ Hz, 1H), 7.29–7.39 (m, 4H), 7.23 (s, 1H), 7.12 (d, $J = 7.6$ Hz, 1H), 7.01 (d, $J = 7.6$ Hz, 1H), 3.89 (s, 2H), 3.85 (s, 2H), 2.54 (s, 3H), 2.10 (s, 1H). ^{13}C NMR (100 MHz, CDCl_3 , 298 K): δ 159.1, 158.1, 140.4, 136.8, 128.5, 128.4, 127.1, 121.6, 119.3, 54.8, 53.7, 24.6. FTIR (KBr, cm^{-1}): 3318 (ν (N-H)), 3062, 3027, 2920, 2837, 1593, 1577, 1456, 1155, 1118, 1028, 780, 742. HRMS-ESI (m/z): $[\text{M} + \text{H}]^+$ calcd for $\text{C}_{14}\text{H}_{17}\text{N}_2$, 213.1392; found, 213.1385.

Synthesis of ferrous chloride complexes

2-(1-(Triphenylmethylamino)methyl)pyridylferrous chloride, Fe1_H. In a glovebox, to a solution of ligand **L1_H** (200 mg, 0.57 mmol) in CH_2Cl_2 (10 mL), anhydrous FeCl_2 (72.3 mg, 0.57 mmol) was added. The resulting suspension was stirred for 48 h at room temperature. The precipitate was collected by filtration under an argon atmosphere, washed with distilled hexane (10 mL \times 2) and dried under vacuum to afford **Fe1_H** as a gray white solid (223.0 mg, 82% yield). ATR-IR (cm^{-1}): 3296 (ν (N-H)), 3053, 1613, 1488, 1446, 1163, 1029, 976, 904, 870, 774, 735, 705. HRMS (ESI, m/z): $[\text{M} - \text{FeCl}_2 + \text{H}]^+$ calcd for $\text{C}_{50}\text{H}_{45}\text{Cl}_2\text{FeN}_4$, 827.2371; found, 827.2386. Anal. calcd for $\text{C}_{25}\text{H}_{22}\text{Cl}_2\text{FeN}_2$: C 62.92, H 4.65, N 5.87; found: C 61.83, H 4.69, N 5.80.

2-(1-(Diphenylmethylamino)methyl)pyridylferrous chloride, Fe2_H. Using the same procedure and molar ratio of reactants as described for **Fe1_H**, but ligand **L2_H** was used instead of **L1_H**, **Fe2_H** was obtained as a white powder (228.0 mg, 79% yield). ATR-IR (cm^{-1}): 3209 (ν (N-H)), 3030, 2870, 1607, 1475, 1445, 1283, 1153, 1040, 984, 943, 810, 774, 766. HRMS (ESI, m/z): $[\text{M} - \text{FeCl}_2 + \text{H}]^+$ calcd for $\text{C}_{38}\text{H}_{37}\text{Cl}_2\text{FeN}_4$, 675.1745; found, 675.1735. Anal. calcd for $\text{C}_{19}\text{H}_{18}\text{Cl}_2\text{FeN}_2$: C 56.89, H 4.52, N 6.98; found: C 56.85, H 4.66, N 7.05.

2-Methyl-6-(1-(diphenylmethylamino)methyl) pyridylferrous chloride, Fe3_{Me}. Using the same procedure and molar ratio of reactants as described for **Fe1_H**, but ligand **L3_{Me}** was used instead of **L1_H**, **Fe3_{Me}** was obtained as a white powder (236.0 mg, 82% yield). ATR-IR (cm^{-1}): 3193 (ν (N-H)), 1606, 1578, 1494, 1466, 1454, 1433, 1383, 1169, 1083, 1032, 1019, 989, 939, 819, 790, 750. HRMS (ESI, m/z): $[\text{M} - \text{FeCl}_2 + \text{H}]^+$ calcd for $\text{C}_{40}\text{H}_{41}\text{Cl}_2\text{FeN}_4$, 703.2058; found, 703.2051. Anal. calcd for $\text{C}_{20}\text{H}_{20}\text{Cl}_2\text{FeN}_2$: C 57.86, H 4.86, N 6.75; found: C 57.09, H 4.87, N 6.47.

2-(1-(1-Phenylethylamino)methyl)pyridylferrous chloride, Fe4_H. Using the same procedure and molar ratio of reactants as described for **Fe1_H**, but ligand **L4_H** was used instead of **L1_H**, **Fe4_H** was obtained as a yellow powder (160.0 mg, 50% yield). ATR-IR (cm^{-1}): 3247 (ν (N-H)), 3026, 1954, 1606, 1571, 1487, 1430, 1383, 1293, 1152, 1077, 1042, 1021, 961, 855, 762. HRMS (ESI, m/z): $[\text{M} - \text{FeCl}_2 + \text{H}]^+$ calcd for $\text{C}_{28}\text{H}_{33}\text{Cl}_2\text{FeN}_4$, 551.1432; found, 551.1445. Anal. calcd for $\text{C}_{14}\text{H}_{16}\text{Cl}_2\text{FeN}_2$: C 49.60, H 4.76, N 8.26; found: C 48.82, H 4.83, N 8.30.

2-(1-(Phenylmethylamino)methyl)pyridylferrous chloride, Fe5_H. Using the same procedure and molar ratio of reactants as described for **Fe1_H**, but ligand **L5_H** was used instead of **L1_H**, **Fe5_H** was obtained as a yellow powder (270.0 mg, 83% yield). ATR-IR (cm^{-1}): 3250 (ν (N-H)), 3026, 2942, 1605, 1571, 1488, 1442, 1335, 1306, 1149, 1088, 1021, 995, 912, 880, 765. HRMS (ESI, m/z): $[\text{M} - \text{FeCl}_2 + \text{H}]^+$ calcd for $\text{C}_{26}\text{H}_{29}\text{Cl}_2\text{FeN}_4$, 523.1119; found, 523.1122. Anal. calcd for $\text{C}_{13}\text{H}_{14}\text{Cl}_2\text{FeN}_2 \cdot 1/4\text{CH}_2\text{Cl}_2$: C 45.96, H 4.22, N 8.09; found: C 45.70, H 4.35, N 8.49.

2-(1-(1-Methylethylamino)methyl)pyridylferrous chloride, Fe6_H. Using the same procedure and molar ratio of reactants as described for **Fe1_H**, but ligand **L6_H** was used instead of **L1_H**, **Fe6_H** was obtained as a yellow powder (240.0 mg, 87% yield). ATR-IR (cm^{-1}): 3241 (ν (N-H)), 2968, 2931, 1605, 1571, 1486, 1444, 1388, 1322, 1291, 1151, 1139, 1101, 1055, 1026, 985, 971, 908, 857, 815, 766. HRMS (ESI, m/z): $[\text{M} - \text{FeCl}_2 + \text{H}]^+$ calcd for $\text{C}_{18}\text{H}_{29}\text{Cl}_2\text{FeN}_4$, 427.1119; found, 427.1108. Anal. calcd for $\text{C}_9\text{H}_{14}\text{Cl}_2\text{FeN}_2$: C 39.03, H 5.10, N 10.11; found: C 38.75, H 5.15, N 9.52.

2-(1-(Cyclohexylamino)methyl)pyridylferrous chloride, Fe7_H. Using the same procedure and molar ratio of reactants as described for **Fe1_H**, but ligand **L7_H** was used instead of **L1_H**, **Fe7_H** was obtained as a yellow powder (250.0 mg, 66% yield). ATR-IR (cm^{-1}): 3245 (ν (N-H)), 2939, 2846, 1604, 1572, 1483, 1450, 1384, 1293, 1239, 1159, 1102, 1091, 1012, 995, 978, 932, 903, 895, 842, 771, 732. HRMS (ESI, m/z): $[\text{M} - \text{FeCl}_2 + \text{H}]^+$ calcd for $\text{C}_{24}\text{H}_{37}\text{Cl}_2\text{FeN}_4$, 507.1745; found, 507.1754. Anal. calcd for $\text{C}_{12}\text{H}_{18}\text{Cl}_2\text{FeN}_2$: C 45.46, H 5.72, N 8.84; found: C 45.19, H 5.76, N 8.83.

2-(1-(4-Methoxyphenylmethylamino)methyl)pyridylferrous chloride, Fe8_H. Using the same procedure and molar ratio of reactants as described for **Fe1_H**, but ligand **L8_H** was used instead of **L1_H**, **Fe8_H** was obtained as a yellow powder (170.0 mg, 61% yield). ATR-IR (cm^{-1}): 3249 (ν (N-H)), 2939, 2836, 2354, 1698, 1610, 1572, 1513, 1486, 1441, 1324, 1301, 1251, 1180, 1050, 1032, 994, 899, 815, 765. HRMS (ESI, m/z): $[\text{M} - \text{FeCl}_2 + \text{H}]^+$ calcd for $\text{C}_{28}\text{H}_{33}\text{Cl}_2\text{FeN}_4\text{O}_2$, 583.1331; found,

Table 4 Crystal data and structure refinement for Fe3_{Me}, Fe4_H, Fe7_H and Fe11_{Me}

	Fe3 _{Me}	Fe4 _H	Fe7 _H	Fe11 _{Me}
Formula	C ₂₀ H ₂₀ Cl ₂ FeN ₂	C ₂₈ H ₃₂ Cl ₄ Fe ₂ N ₄	(C ₁₂ H ₁₈ Cl ₂ FeN ₂) _n	C ₁₄ H ₁₆ Cl ₂ FeN ₂
Formula weight	415.13	678.08	317.03 <i>n</i>	339.04
Temperature/K	298(2)	298(2)	293(2)	298(2)
Crystal system	Triclinic	Monoclinic	Orthorhombic	Monoclinic
Space group	<i>P</i> $\bar{1}$	<i>C2/c</i>	<i>Pbca</i>	<i>P2₁/c</i>
<i>a</i> /Å	8.9981(8)	15.1785(13)	9.1540(8)	7.0439(7)
<i>b</i> /Å	10.7524(9)	9.3366(8)	6.8673(6)	13.0684(11)
<i>c</i> /Å	11.3021(11)	22.6274(18)	42.281(3)	16.9522(12)
α /°	89.495(3)	90	90	90
β /°	66.7300(10)	103.782(2)	90	90.7610(10)
γ /°	79.902(2)	90	90	90
<i>V</i> /Å ³	986.77(15)	3114.3(5)	2657.9(4)	1560.4(2)
<i>Z</i>	2	4	8	4
<i>D</i> _{calc} /Mg m ⁻³	1.397	1.446	1.585	1.443
Absorption coefficient/mm ⁻¹	1.04	1.30	12.62	1.30
<i>F</i> (000)	428	1392	1312	696
Crystal size/mm	0.22 × 0.15 × 0.10	0.16 × 0.11 × 0.10	0.30 × 0.15 × 0.05	0.48 × 0.42 × 0.40
θ limits/°	3.8–22.4	2.5–25.0	4.2–66.1	2.4–25.0
Reflections collected/unique	5011/3435	7713/2739	13 972/2242	7388/2760
<i>R</i> ^{int}	0.048	0.038	0.115	0.029
Goodness of fit on <i>F</i> ²	1.011	1.04	1.09	1.06
Final <i>R</i> indices [<i>I</i> > 2 σ (<i>I</i>)]	<i>R</i> ₁ = 0.0539 <i>wR</i> ₂ = 0.1171	<i>R</i> ₁ = 0.034 <i>wR</i> ₂ = 0.066	<i>R</i> ₁ = 0.099 <i>wR</i> ₂ = 0.223	<i>R</i> ₁ = 0.035 <i>wR</i> ₂ = 0.092
<i>R</i> indices (all data)	<i>R</i> ₁ = 0.0804 <i>wR</i> ₂ = 0.1264	<i>R</i> ₁ = 0.059 <i>wR</i> ₂ = 0.072	<i>R</i> ₁ = 0.1370 <i>wR</i> ₂ = 0.2580	<i>R</i> ₁ = 0.0570 <i>wR</i> ₂ = 0.092

583.1343. Anal. calcd for C₁₄H₁₆Cl₂FeN₂O·1/4CH₂Cl₂: C 45.49, H 4.42, N 7.45; found: C 45.74, H 4.55, N 7.91.

2-(1-(4-Trifluoromethylphenylmethylamino)methyl)pyridylferrous chloride, Fe9_H. Using the same procedure and molar ratio of reactants as described for Fe1_H, but ligand L9_H was used instead of L1_H, Fe9_H was obtained as a yellow powder (241.0 mg, 82% yield). ATR-IR (cm⁻¹): 3251 (ν (N-H)), 2941, 1606, 1571, 1436, 1329, 1164, 1115, 1066, 1020, 986, 900, 815, 765. HRMS (ESI, *m/z*): [M – FeCl₃]⁺ calcd for C₂₈H₂₆ClF₆FeN₄, 623.1100; found, 623.1107. Anal. calcd for C₁₄H₁₃Cl₂F₃FeN₂: C 42.79, H 3.33, N 7.13; found: C 42.46, H 3.27, N 7.25.

2-(1-(2,4,6-Trimethylphenylmethylamino)methyl)pyridylferrous chloride, Fe10_H. Using the same procedure and molar ratio of reactants as described for Fe1_H, but ligand L10_H was used instead of L1_H, Fe10_H was obtained as a yellow powder (160.0 mg, 70% yield). ATR-IR (cm⁻¹): 3290 (ν (N-H)), 2979, 2948, 1608, 1573, 1486, 1441, 1363, 1312, 1151, 1080, 1051, 1022, 981, 894, 869, 813, 761. HRMS (ESI, *m/z*): [M – FeCl₂ + H]⁺ calcd for C₃₂H₄₁Cl₂FeN₄, 607.2058; found, 607.2070. Anal. calcd for C₁₆H₂₀Cl₂FeN₂: C 52.35, H 5.49, N 7.63; found: C 51.36, H 5.51, N 7.55.

2-Methyl-6-(1-(phenylmethylamino)methyl)pyridylferrous chloride, Fe11_{Me}. Using the same procedure and molar ratio of reactants as described for Fe1_H, but ligand L11_{Me} was used instead of L1_H, Fe11_{Me} was obtained as a yellow powder (277.0 mg, 87% yield). ATR-IR (cm⁻¹): 3235 (ν (N-H)), 2941, 1608, 1575, 1469, 1340, 1275, 1164, 1094, 1051, 1022, 998, 876, 797, 746. HRMS (ESI, *m/z*): [M – FeCl₂ + H]⁺ calcd for C₂₈H₃₃Cl₂FeN₄, 551.1432; found, 551.1442. Anal. calcd for C₁₄H₁₆Cl₂FeN₂: C 49.60, H 4.76, N 8.26; found: C 48.63, H 4.57, N 8.09.

X-ray crystallographic studies

For complexes Fe3_{Me}, Fe4_H, Fe7_H and Fe11_{Me}, a single crystal suitable for X-ray analysis was sealed into a fine-focus sealed tube, and the intensity data of the single crystal were collected on the CCD-Bruker Smart system. All determinations of the unit cell and intensity data for Fe3_{Me}, Fe4_H and Fe11_{Me} were performed with graphite-monochromated Mo-K α radiation (λ = 0.71073 Å); however, Xcalibur/Gemini was used with Cu-K α radiation (λ = 1.54178 Å) for crystal Fe7_H. The structures were solved by direct methods and refined by full-matrix least-squares on *F*². All hydrogen atoms were placed at calculated positions. Structural solution and refinement were performed using the SHELXL-2018/3.⁷¹ Crystal data and structure refinement for Fe3_{Me}, Fe4_H, Fe7_H and Fe11_{Me} are shown in Table 4.

General procedure for isoprene polymerization

In a typical experiment, a reactor was heated, dried in a vacuum, and recharged with nitrogen three times. When the reactor cooled down, iron(II) complexes (10 μ mol), toluene (5 mL), isoprene (2 mL, 20 mmol) and MAO cocatalyst were added into the reactor in order. The reaction was employed for the corresponding time and was then quenched with a diluted HCl solution of methanol (MeOH/HCl = 50/1). The polymer was collected by filtration and washed with methanol several times and dried at room temperature for 24 h under vacuum until constant weight was reached.

Conflicts of interest

There are no conflicts to declare.

Acknowledgements

Generous support by the Major Science and Technology Innovation Program of Shandong Province (2018CXGC1105), the CAS Hundred Talents Program (Y5100719AL), the Young Taishan Scholars Program of Shandong Province (tsqn201812112), the “135” Projects Fund of CAS-QIBEBT Director Innovation Foundation, DICP& QIBEBT United Foundation (UN201701) and the National Natural Science Foundation of China (21702215) is gratefully acknowledged.

References

- D. Li, S. Li, D. Cui and X. Zhang, *Organometallics*, 2010, **29**, 2186–2193.
- International Rubber Study Group, *Rubber Statistical Bulletin*, 2015.
- S. Li, D. Cui, D. Li and Z. Hou, *Organometallics*, 2009, **28**, 4814–4822.
- G. Zhu, X. Zhang, M. Zhao, L. Wang, C. Jing, P. Wang, X. Wang and Q. Wang, *Polymers*, 2018, **10**, 934.
- J. Wolpers, H. B. Fuchs, C. Herrmann, W. Hellermann, K. H. Nordsiek, H. Fuchs and K. Nordsiek, US5104941-A, 1992.
- H. Liu, J. He, Z. Liu, Z. Lin, G. Du, S. Zhang and X. Li, *Macromolecules*, 2013, **46**, 3257–3265.
- A.-Q. Jia, J.-Q. Wang, P. Hua and G.-X. Jin, *Dalton Trans.*, 2011, **40**, 7730–7736.
- L. K. Johnson, C. M. Killian and M. Brookhart, *J. Am. Chem. Soc.*, 1995, **117**, 6414–6415.
- C. M. Killian, D. J. Tempel, L. K. Johnson and M. Brookhart, *J. Am. Chem. Soc.*, 1996, **118**, 11664–11665.
- B. L. Small, M. Brookhart and A. M. A. Bennett, *J. Am. Chem. Soc.*, 1998, **120**, 4049–4050.
- G. J. P. Britovsek, V. C. Gibson, B. S. Kimberley, P. J. Maddox, S. J. McTavish, G. A. Solan, A. J. P. White and D. J. Williamsa, *Chem. Commun.*, 1998, 849–850.
- Z.-J. Yao and G.-X. Jin, *Coord. Chem. Rev.*, 2013, **257**, 2522–2535.
- S. Zhou and C. Chen, *Sci. Bull.*, 2018, **63**, 441–445.
- J. Fang, X. Sui, Y. Li and C. Chen, *Polym. Chem.*, 2018, **9**, 4143–4149.
- Q. Dai, X. Jia, F. Yang, C. Bai, Y. Hu and X. Zhang, *Polymers*, 2016, **8**, 12.
- F.-S. Liu, H.-B. Hu, Y. Xu, L.-H. Guo, S.-B. Zai, K.-M. Song, H.-Y. Gao, L. Zhang, F.-M. Zhu and Q. Wu, *Macromolecules*, 2009, **42**, 7789–7796.
- D. Peng, X. Yan, C. Yu, S. Zhang and X. Li, *Polym. Chem.*, 2016, **7**, 2601–2634.
- C. Chen, *ACS Catal.*, 2018, **8**, 5506–5514.
- X. Fu, L. Zhang, R. Tanaka, T. Shiono and Z. Cai, *Macromolecules*, 2017, **50**, 9216–9221.
- Y. Na, S. Dai and C. Chen, *Macromolecules*, 2018, **51**, 4040–4048.
- D. Gong, X. Jia, B. Wang, X. Zhang and L. Jiang, *J. Organomet. Chem.*, 2012, **702**, 10–18.
- J. Guo, B. Wang, J. Bi, C. Zhang, H. Zhang, C. Bai, Y. Hu and X. Zhang, *Polymer*, 2015, **59**, 124–132.
- Z. Wang, G. A. Solan, Q. Mahmood, Q. Liu, Y. Ma, X. Hao and W.-H. Sun, *Organometallics*, 2018, **37**, 380–389.
- Q. Mahmood, J. Guo, W. Zhang, Y. Ma, T. Liang and W.-H. Sun, *Organometallics*, 2018, **37**, 957–970.
- Q. Mahmood, E. Yue, J. Guo, W. Zhang, Y. Ma, X. Hao and W.-H. Sun, *Polymer*, 2018, **159**, 124–137.
- Y. Nakayama, Y. Baba, H. Yasuda, K. Kawakita and N. Ueyama, *Macromolecules*, 2003, **36**, 7953–7958.
- D. Gong, B. Wang, C. Bai, J. Bi, F. Wang, W. Dong, X. Zhang and L. Jiang, *Polymer*, 2009, **50**, 6259–6264.
- B. Minaev, A. Baryshnikova and W.-H. Sun, *J. Organomet. Chem.*, 2016, **811**, 48–65.
- R. Gao, L. Xiao, X. Hao, W. H. Sun and F. Wang, *Dalton Trans.*, 2008, 5645–5651.
- J. Zhang, W. Gao, X. Lang, Q. Wu, L. Zhang and Y. Mu, *Dalton Trans.*, 2012, **41**, 9639–9645.
- Y. Zhang, C. Huang, X. Wang, Q. Mahmood, X. Hao, X. Hu, C.-Y. Guo, G. A. Solan and W.-H. Sun, *Polym. Chem.*, 2017, **8**, 995–1005.
- Z. Chen, M. D. Leatherman, O. Daugulis and M. Brookhart, *J. Am. Chem. Soc.*, 2017, **139**, 16013–16022.
- L. Zhong, G. Li, G. Liang, H. Gao and Q. Wu, *Macromolecules*, 2017, **50**, 2675–2682.
- Y. Zeng, Q. Mahmood, T. Liang and W.-H. Sun, *J. Polym. Sci., Part A: Polym. Chem.*, 2017, **55**, 3214–3222.
- Y. Zeng, Q. Mahmood, Q. Zhang, T. Liang and W.-H. Sun, *Eur. Polym. J.*, 2018, **103**, 342–350.
- D. B. Culver, H. Tafazolian and M. P. Conley, *Organometallics*, 2018, **37**, 1001–1006.
- S. Dai and C. Chen, *Macromolecules*, 2018, **51**, 6818–6824.
- L. K. Johnson, C. M. Killian and M. Brookhart, *J. Am. Chem. Soc.*, 1995, **117**, 6414–6415.
- B. L. Small and M. Brookhart, *J. Am. Chem. Soc.*, 1998, **120**, 7143–7144.
- G. Ricci, A. Sommazzi, F. Masi, M. Ricci, A. Boglia and G. Leone, *Coord. Chem. Rev.*, 2010, **254**, 661–676.
- X. Jiang, X. Wen, W.-H. Sun and A. He, *J. Polym. Sci., Part A: Polym. Chem.*, 2014, **52**, 2395–2398.
- X. Wang, L. Fan, C. Huang, T. Liang, C.-Y. Guo and W.-H. Sun, *J. Polym. Sci., Part A: Polym. Chem.*, 2016, **54**, 3609–3615.
- M. N. Alnajrani, S. A. Alshimiri and O. A. Alsager, *RSC Adv.*, 2016, **6**, 113803–113814.
- J. Raynaud, J. Y. Wu and T. Ritter, *Angew. Chem.*, 2012, **51**, 11805–11808.
- L. Guo, X. Jing, S. Xiong, W. Liu, Y. Liu, Z. Liu and C. Chen, *Polymers*, 2016, **8**, 389.
- H. Liu, S. Yang, F. Wang, C. Bai, Y.-m. Hu and X. Zhang, *Chin. J. Polym. Sci.*, 2016, **34**, 1060–1069.
- G. Ricci, D. Morganti, A. Sommazzi, R. Santi and F. Masi, *J. Mol. Catal. A: Chem.*, 2003, **204–205**, 287–293.
- C. Bazzini, A. Giarrusso, L. Porri, B. Pirozzi and R. Napolitano, *Polymer*, 2004, **45**, 2871–2875.

- 49 G. J. P. Britovsek, S. P. D. Baugh, O. Hoarau, V. C. Gibson, D. F. Wass, A. J. P. White and D. J. Williams, *Inorg. Chim. Acta*, 2003, **345**, 279–291.
- 50 X. Feng, J.-G. Wang, C.-Z. Xie and N. Ma, *Z. Anorg. Allg. Chem.*, 2007, **633**, 2085–2088.
- 51 X. Zhang, G. Zhu, Q. Mahmood, M. Zhao, L. Wang, C. Jing, X. Wang and Q. Wang, *J. Polym. Sci., Part A: Polym. Chem.*, 2019, **57**, 767–775.
- 52 M. Zhao, L. Wang, Q. Mahmood, C. Jing, G. Zhu, X. Zhang, X. Wang and Q. Wang, *Appl. Organomet. Chem.*, 2019, **33**, e4836.
- 53 T. Zheng, H. Liao, J. Gao, L. Zhong, H. Gao and Q. Wu, *Polym. Chem.*, 2018, **9**, 3088–3097.
- 54 Z. Huang, K. Song, F. Liu, J. Long, H. Hu, H. Gao and Q. Wu, *J. Polym. Sci., Part A: Polym. Chem.*, 2008, **46**, 1618–1628.
- 55 S. Zai, H. Gao, Z. Huang, H. Hu, H. Wu and Q. Wu, *ACS Catal.*, 2012, **2**, 433–440.
- 56 Z. Chen, J.-F. Li, W.-J. Tao, X.-L. Sun, X.-H. Yang and Y. Tang, *Macromolecules*, 2013, **46**, 2870–2875.
- 57 D.-W. Wan, Z. Chen, Y.-S. Gao, Q. Shen, X.-L. Sun and Y. Tang, *J. Polym. Sci., Part A: Polym. Chem.*, 2013, **51**, 2495–2503.
- 58 X. H. Yang, C. R. Liu, C. Wang, X. L. Sun, Y. H. Guo, X. K. Wang, Z. Wang, Z. Xie and Y. Tang, *Angew. Chem., Int. Ed.*, 2009, **48**, 8099–8102.
- 59 B. C. K. Chan and M. C. Baird, *Inorg. Chim. Acta*, 2004, **357**, 2776–2782.
- 60 V. C. Gibson, R. K. O'Reilly, D. F. Wass, A. J. P. White and D. J. Williams, *Dalton Trans.*, 2003, 2824–2830.
- 61 Y. Matsubara, T. Yamaguchi, T. Hashimoto and Y. Yamaguchi, *Polyhedron*, 2017, **128**, 198–202.
- 62 J. Gao, B. Yang and C. Chen, *J. Catal.*, 2019, **369**, 233–238.
- 63 B. K. Long, J. M. Eagan, M. Mulzer and G. W. Coates, *Angew. Chem.*, 2016, **128**, 7222–7226.
- 64 D. Liu, D. Cui and W. Gao, *Sci. China: Chem.*, 2010, **53**, 1641–1645.
- 65 B. Wang, D. Cui and K. Lv, *Macromolecules*, 2008, **41**, 1983–1988.
- 66 P. Hu, Y.-L. Qiao, J.-Q. Wang and G.-X. Jin, *Organometallics*, 2012, **31**, 3241–3247.
- 67 G. Ricci, G. Leone, A. Boglia, A. C. Boccia and L. Zetta, *Macromolecules*, 2009, **42**, 9263–9267.
- 68 B. Liu, X. Wang, Y. Pan, F. Lin, C. Wu, J. Qu, Y. Luo and D. Cui, *Macromolecules*, 2014, **47**, 8524–8530.
- 69 L. Annunziata, S. Pragliola, D. Pappalardo, C. Tedesco and C. Pellecchia, *Macromolecules*, 2011, **44**, 1934–1941.
- 70 S. J. Dickson, M. J. Paterson, C. E. Willans, K. M. Anderson and J. W. Steed, *Chem. – Eur. J.*, 2008, **14**, 7296–7305.
- 71 G. M. Sheldrick, *Acta Crystallogr., Sect. C: Struct. Chem.*, 2015, **71**, 3–8.